In this issue

European Centre for Medium-Range Weather Forecasts

Shinfield Park, Reading, Berkshire RG2 9AX, UK

Fax: . . . . . .+44 118 986 9450

Telephone: National. 0118 949 9000

International . . . . . +44 118 949 9000

Public Web site . . . . . http://www.ecmwf.int

Member States' Web site . . . . . http://wms.ecmwf.int

Editorial

Details of recent improvements to the operational forecasting system that were introduced during the autumn in IFS cycle CY21r4 are described in the article on page 2. The changes allow better use of observations in the assimilation, better analyses of low-level winds, improved vertical structure in the tropics, more realistic orography fields, and improved forecasts of precipitation, 10 m wind speed, low-level cloud and relative humidity. The anomaly correlation scores during the test period indicated substantial improvements in forecasting accuracy, especially over Europe and the Northern Hemisphere.

Anna Ghelli describes the problem of verifying precipitation predictions by comparing grid-scale model forecasts with observations at single locations on page 9. She suggests that a more appropriate approach is to use grid-box averages of the observations (or 'super-observations') as the baseline 'truth' for the forecast verification.

Dieter Niebel gives an overview of the features of ECMWF's new local area network on page 17. The new LAN provides improved bandwidth and reliability, and increased port density for the desktops and servers.

Changes to the Operational Forecasting System

Recent changes

On 11 April 2000, a new version of the operational model was implemented (cycle 22r1). This is a minor scientific upgrade that includes:

- a revised use of SSM/I radiances including a bias correction and preventing the assimilation of radiances where precipitation occurs; both satellites (DMSP-13 and 14) are now used;
- a modification to the assimilation of humidity in the stratosphere to avoid the unrealistic moistening that has been occurring since the last model change (12 October 1999).

A technical change has also been brought in through the use of a new postprocessing software (Full-Pos) developed in collaboration with Météo-France. This change will allow the introduction of new parameters in the dissemination and MARS archive, details of which will be announced later.

This new version of the model is running on the new Fujitsu VPP5000 computer.

François Lalaurette

The IFS cycle CY21r4 made operational in October 1999

On 12 October 1999 a substantial set of modifications to both the forecast model and the data assimilation system were introduced as the operational cycle (IFS cycle CY21r4). This article provides an overview over these changes, some of which are the result of several years of development. It is shown that the introduction of this new cycle has resulted in substantial improvements to the forecasting system. The changes that were introduced in CY21r4 are:

Data assimilation

- revisions to the background error statistics used in the 4D-Var system;
- revisions to the bias correction scheme for TOVS/ATOVS radiances;
- correction of the analysis of humidity from conventional data sources;
- the introduction of the assimilation of 10 m winds from the SSM/I instrument.

Model

- an increase in the number of model levels to 60, allowing higher vertical resolution, mainly in the planetary boundary layer;
- revisions to the cloud and convection schemes;
- improved fields for orography, land-sea mask, and the subgrid-scale orography scheme;
- revisions to the post-processing of 10 m wind.

These changes are discussed below and their major impacts highlighted. More detail on many of the modifications can be found in the papers listed at the end of this article and in ECMWF Research Department Technical Memoranda, which can be made available on request.

Data assimilation changes

New background error statistics

The technique used to derive the statistics of background (or first guess) errors is one of the most important aspects of any analysis system. To a large extent, these statistics determine the way in which information provided by the observations is interpolated and extrapolated to the model's grid points.

Since 1997, the ECMWF analysis has modelled the background error statistics by applying a sequence of steps that attempt to transform the model fields to a form in which the background errors have unit variance and are uncorrelated. The covariance matrix for errors in these transformed fields is simply the identity matrix, and the background cost function is consequently easy to evaluate. Each step of the transformation (often called the 'change of variable') requires the application of matrices or operators whose coefficients are determined empirically. The coefficients were derived using the so-called NMC method from a large sample of differences between pairs of forecasts of different duration verifying on the same date (pairs of 48-hour and 24-hour forecasts were used). The sample of forecast differences provided a surrogate for a sample of background errors.

For CY21r4, the overall structure of the change of variable has been retained. However, the way in which the coefficients are calculated is different. An 'ensemble' of independent analysis experiments was conducted, each producing analyses for the period 3-28 February 1999 but which differed from one another because, for each experiment, the observations were randomly perturbed by an amount typical of the assumed observation errors. It can be shown that, if the model were perfect and the analysis system linear, and if the perturbations applied to the observations were statistically similar to the true observation errors, then the difference between any pair of background fields verifying at the same time would represent a sample from the distribution of background error. Differences between pairs of backgrounds produced in this way were used instead of forecast differences to calculate the background error statistics for the CY21r4 assimilation system. In order to remove the assumption of a perfect model, a representation of the effects of model error was included by perturbing the model during the first-guess forecasts using a 'stochastic physics' method.

The most obvious difference between the background statistics derived from the analysis ensemble and those calculated using the NMC method is that the former statistics have shorter horizontal and vertical correlation length scales. An illustration of this is given in Figure 1, which shows wave-number averaged vertical correlation matrices for vorticity background errors calculated by the two methods. The NMC method gives much deeper vertical correlations, particularly in the middle-to-upper troposphere.

Revised bias correction of TOVS/ATOVS radiances

In the past, the RTOVS bias correction files were recalculated every month. A new method, using model predictors, was introduced in IFS-cycle CY18r6 and, because it became clear that the bias correction produced in this way was more stable, the updating period was extended to about two months. When ATOVS 1C radiances replaced RTOVS the IFS-cycle CY21r1 used a bias correction computed 4 months earlier. Prior to the introduction of CY21r4, an extensive review was undertaken of the bias correction procedures, taking into account the new stratospheric levels that had been introduced in the earlier 50-level model and the availability of data from the new AMSU instrument. As a result it was decided to use six model predictors and to revise the geographical sample-matching and statistical screening. The new procedure was tested with the CY21r4 model and was shown to improve the forecast performance of the system.

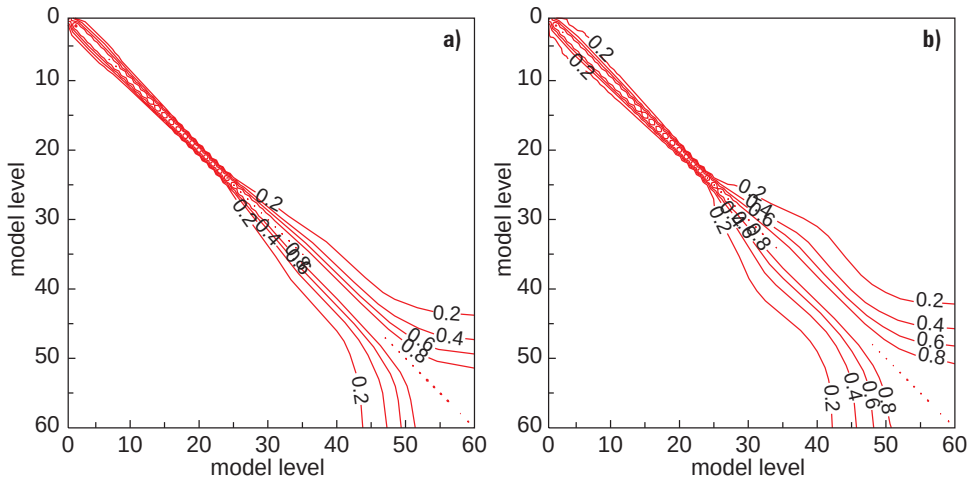

Figure 1: Wave-number averaged vertical correlation matrix for vorticity background errors calculated using (a) the new method and (b) the NMC method. Model levels 30, 39 and 49 are near pressure levels 200 hPa, 500 hPa and 850 hPa, respectively. The vertical correlation length scales are shorter in (a), especially in the middle and upper troposphere.

Correction of the humidity analysis

SYNOP and radiosonde humidity observations are received in the form of dew-point temperature data. For ease of use in the data assimilation, these data are converted to either relative humidity (SYNOP) or specific humidity (sondes). However, the way that this conversion has been done for many years at ECMWF has not followed WMO guidelines. The conversion ought to be done using the saturation vapour pressure calculated with respect to water at all levels in the atmosphere, without involvement of ice or mixed ice/water phases. However, prior to CY21R4, the conversion had been done using the model's definition of saturation vapour pressure, which allows for ice and mixed phases. The use of the correct procedure leads to an apparent increase in measured humidity, especially where the relative humidity is high and the temperature is far below freezing. In areas with good radiosonde data-coverage, the effect on data assimilation is a substantial moistening of the upper troposphere. In zonal-mean terms the CY21r4 analyses are between 6% and 12% moister than those produced by the previous scheme, especially in the 500-300 hPa layer north of 40°N, as shown in Figure 2. In the tropics, and in the Southern Hemisphere, the area-averaged impact is much smaller due to the lesser density of the radiosonde network.

With the corrected treatment of humidity observations there is a better agreement between observed and model humidity, and this results in reduced humidity analysis increments in the assimilation. Previously the observations appeared to be biased dry in the upper troposphere compared with the model, whereas now they appear to be largely unbiased. The increased moisture has also affected the amount of high cloud in the model, with an increase from around 27% to 32% cloudiness in the Northern Hemisphere mid and high latitudes. The forecast impact was tested over the 40-day period from 26 July to 4 September 1999, and there was a surprisingly large and positive improvement for the Northern Hemisphere troposphere.

Over a timescale of several weeks the test assimilation increased moisture in the lower stratosphere in high and mid latitudes. In subsequent operational use, the lower-stratospheric humidity became quite unrealistically high, leading to significant systematic forecast errors in temperature and eddy kinetic energy. A cure for this side effect of the corrected treatment of humidity observations has been implemented in IFS cycle CY22r1. The operational analyses produced from 12 October 1999 to April 2000 with CY21r4 must, however, be regarded as being unsuitable for use in studies of local stratospheric humidity.

The post-processing of the 2 m dewpoint has also been changed to reflect WMO guidelines for observing and reporting, i.e. to use saturation vapour pressure with respect to water only (N.B. users of the analysed and forecast 2 m temperature and dewpoint to infer near-surface relative or specific humidity will need to change their procedures accordingly).

10 m winds from SSM/I

Estimates of total column water vapour derived by a one-dimensional variational analysis (1D-Var) of SSM/I radiance data have been assimilated operationally at ECMWF since 29 June 1998. The 1D-Var also produces estimates of surface wind speed over the sea; these have been monitored for some time and have been found to be of good quality. Consequently, experiments have been conducted to test the impact of assimilating these SSM/I wind speed estimates in the ECMWF 4D-Var analysis system. Using data from the DMSP-F13 spacecraft, it has been found that the assimilation of the SSM/I wind speed estimates generally increases the model surface wind. The largest changes are found over the southern oceans in winter where the SSM/I data cause mean wind speed increases of up to 0.5 m/s over large areas. Smaller, but still significant, wind speed increases are found over the North Atlantic and North Pacific in winter. The systematic changes to the analysis have resulted in a better agreement with conventional marine wind observations (from ships and buoys), but have also improved the analysis fit to independent (i.e. not assimilated) ERS-2 altimeter data (Figure 3). Furthermore, a number of cases have arisen when the use of the SSM/I wind speed data has had a major synoptic impact upon the analysis and has produced significantly improved medium-range

forecasts. As a result of these tests, the SSM/I wind speed estimates are now assimilated operationally in the CY21r4 system.

Model changes

Vertical resolution

The impact of the increased stratospheric vertical resolution introduced with the earlier 50-level version of the model has been described in a Newsletter article by Untch *et al.* (ECMWF Newsletter No. 82, Winter 98/99, pp. 2–8). The increased number of levels to 60 in the CY21r4 model doubles the vertical resolution below 1500 m; adequate vertical resolution in the lower troposphere has been shown to be fundamental for the proper representation and prediction of boundary-layer processes. This brings the lowest model level down to 10 m above the surface compared with 33 m in the previous 50-level model. Other consequences of the new vertical resolution are that the level of poorest vertical resolution moves up from about 730 hPa to 575 hPa, and there are three additional model levels above 850 hPa in the troposphere and one additional level in the stratosphere.

A schematic of the distribution of levels for the L50 and L60 versions from the surface to 700 hPa (where the largest increase in resolution is located) is shown in Figure 4. In long integrations (120 days), the low-cloud cover in the L60 configuration has generally increased relative to the L50 model, particularly over the stratocumulus areas and the southern ocean – an improvement according to ISCCP observations. The L60 model also produces more realistic precipitation fields in the oceanic equatorial regions.

L60 and L50 assimilation experiments have also been performed for two periods in winter and summer. The L60 model fits the TEMP humidity observations better than the L50 model globally, and a positive impact from the L60 version is also clear from the statistics of the tropical TEMP temperature observation increments in the troposphere.

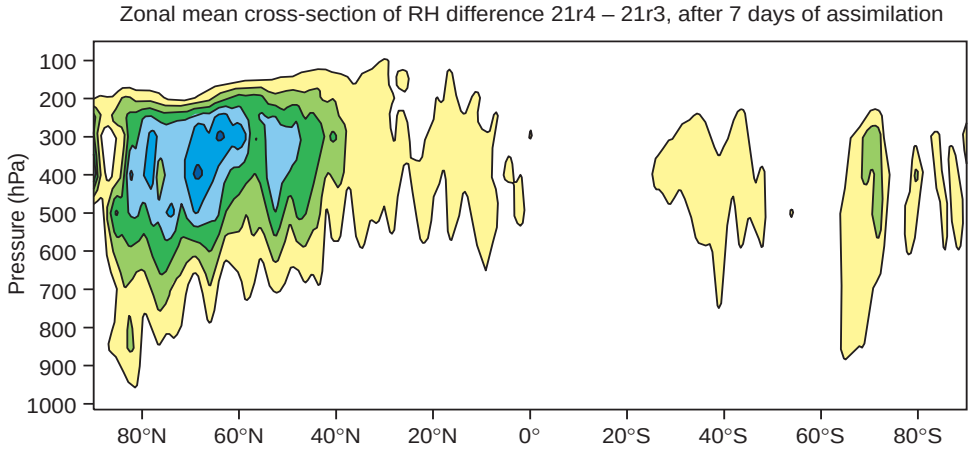

Figure 2: Relative-humidity differences after 7 days of assimilation between systems with and without the correct procedure for converting radiosonde and surface humidity observations. Note the apparent increase in humidity in the upper troposphere in regions of relatively dense radiosonde observations.

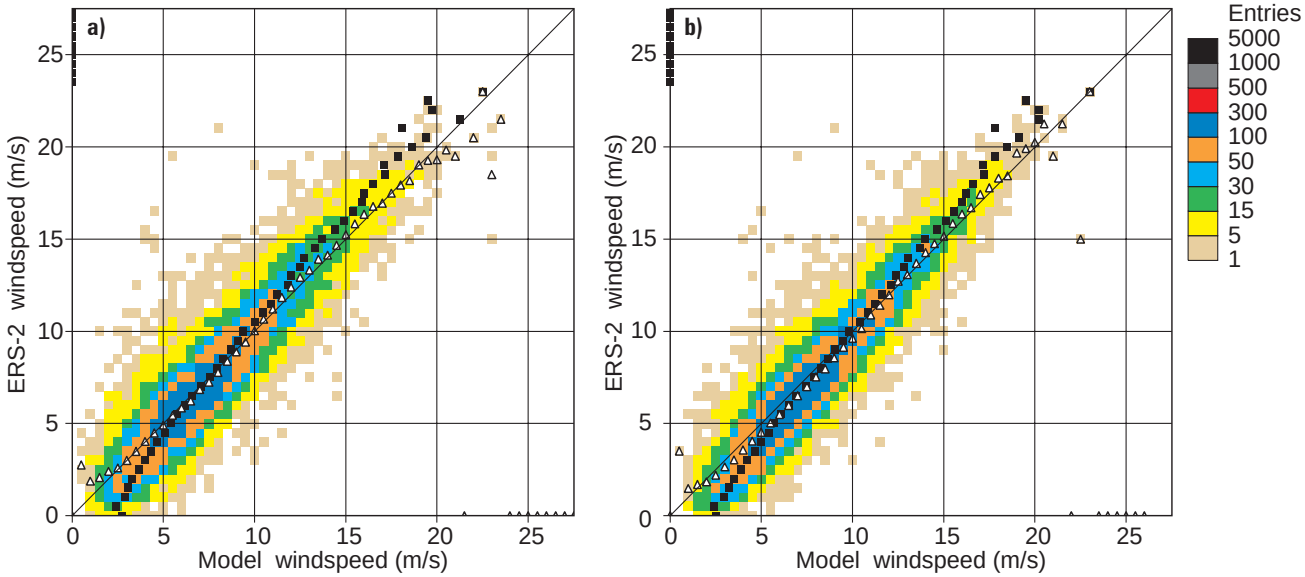

Figure 3: Fit of analysed 10 m wind to ERS-2 altimeter data for analyses from 1500 UTC 15 September 1998 to 0900 UTC 30 September 1998 when (a) the SSM/I wind speed estimates are assimilated, and (b) when they are not. The use of the SSM/I winds in the analysis reduces the wind bias from -0.35 m/s to -0.03 m/s.

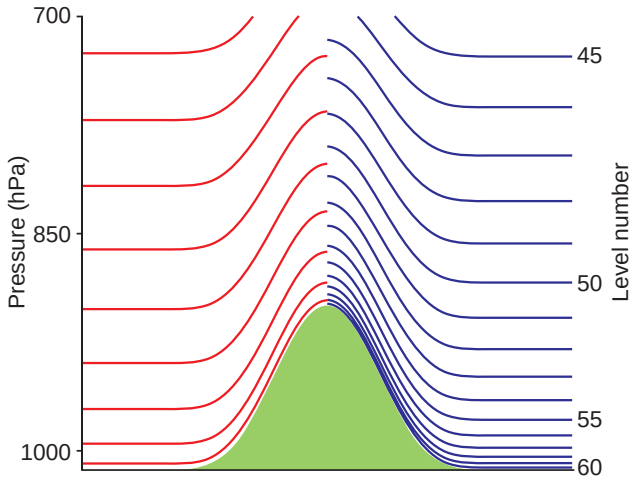

Figure 4: The distribution of model levels below 700 hPa for the 50-level (left) and 60-level (right) versions of the ECMWF model.

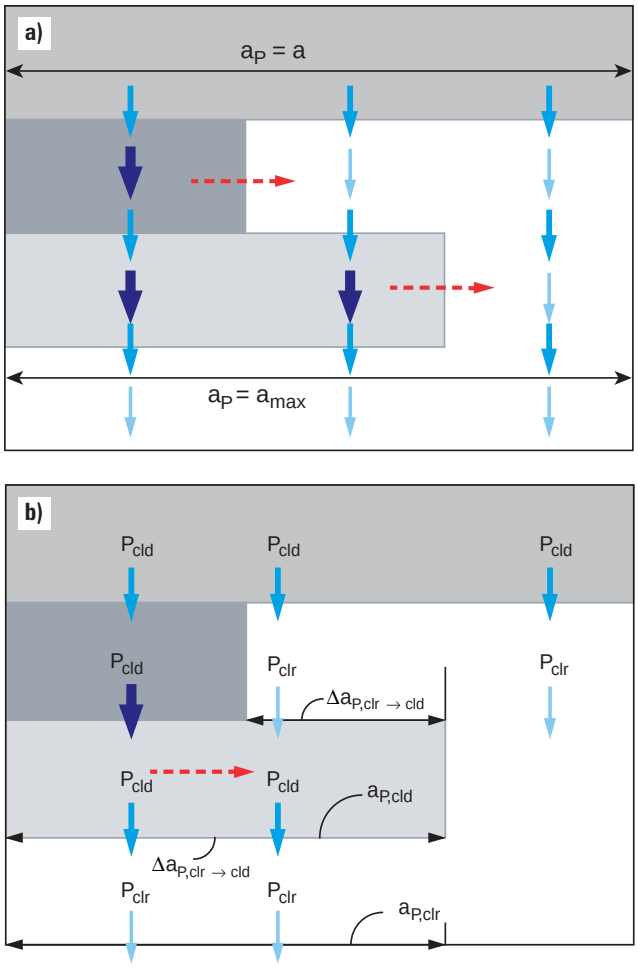

Figure 5: Schematic of the treatment of cloud and precipitation overlap in (a) the old cloud parametrization and (b) the new cloud parametrization. The vertical arrows denote falling precipitation, with P_{cld} and P_{clr} signifying the precipitation in the cloudy and clear regions, respectively. The horizontal dashed arrows indicate the apparent transfer of water arising as a consequence of the averaging process.

Cloud and convection scheme changes

A large number of changes to both the cloud and the convection parametrization have been introduced into the CY21r4 operational model. At the heart of the changes to the cloud scheme is a revision of the treatment of precipitation. In previous versions of the ECMWF model, as in most other GCMs, precipitation was described by using a grid-mean flux, with a possible separation into rain and snow. Recent research has identified serious shortcomings in this approach if the fractional area covered by clouds within a grid box varies with height. The main reason for this is illustrated in Figure 5(a), which shows four model layers, three of which are covered by clouds of various sizes (grey boxes). Precipitation is generated in the top cloud level. As it falls into the layer below, part of it enters cloud and part falls into clear sky. The part inside the cloud will be enhanced due to conversion and/or collection processes whereas, outside the cloud, precipitation will evaporate. If only the grid-mean flux is used to describe precipitation, the two very different precipitation fluxes (large inside cloud, small outside cloud) need to be averaged before entering the next layer. This implies a horizontal water transport from cloud into clear sky (indicated by a dashed horizontal arrow). Due to this transport, more precipitation is available for evaporation in the clear-sky part of the next model layer. This has been shown to lead to a substantial overestimation of evaporation in the presence of vertically varying cloud fraction. In order to address the problems outlined here, a new treatment of precipitation has been developed that separates precipitation fluxes into cloudy and clear-sky contributions, in a very similar way to the treatment of radiative fluxes in cloudy columns. The basic principle of this scheme is illustrated in Figure 5(b). The separation of cloudy and clear-sky precipitation avoids the averaging problems between the two parts of the grid box, although averaging within each of the two portions of the grid is still necessary (as indicated in the cloudy part of the third layer from the top in Figure 5(b)). However, the effects of this averaging are small compared with averaging between cloud and clear sky. An interesting "by-product" of this new treatment of precipitation is a prediction of what fraction of the grid box is covered by precipitation (often referred to as the precipitation fraction). The availability of this product opens up new possibilities for precipitation forecasting and validation, and these are currently under investigation.

For brevity, all other changes to the cloud parametrization are only listed here. They consist of:

- a revised treatment of the cloud sources due to convection;
- a revised treatment of stratiform cloud generation;
- a separation of small and large ice particles in the description of ice sedimentation;
- the introduction of an implicit numerical scheme for precipitation evaporation;
- a change to the treatment of threshold relative humidity above which no precipitation evaporation takes place;

- an increase in cloud erosion in shallow cumulus clouds;
- a revised treatment of the pure-ice mixed-phase transition layer.

Various modifications to the convection parametrization have also been introduced into the new model. They are:

- an increase of the relaxation timescale in the closure for deep convection to a minimum value of one hour at horizontal resolutions higher than TL159;
- a reduction in the strength of the penetration of the tropical tropopause by deep convective updraughts;
- an enhancement of the conversion from liquid water to precipitation by a factor of 1.3.

New orography fields

Global model orography, land-sea mask, and subgrid-scale orography fields have been created for each model resolution from a more detailed orography and land-cover dataset. The so-called USNAVY dataset containing terrain height and percentage of land at 10' x 10' resolution (about 15 km) was used to generate these fields which were included in the operational model from 1 April 1981 to 1 April 1998. Subsequently, for CY18r5 and later cycles, the global orography and land-sea mask (but not the subgrid orography fields) were calculated from a new 2'30" x 2'30" dataset created by Météo-France in co-operation with ECMWF. In CY21r4, a further change has been made to use a newer dataset for terrain heights at a finer resolution of 30" x 30" (GTOPO30), together with a dataset for land cover with similar resolution, i.e. about 1 km global resolution. The GTOPO30 data, distributed by the US Geological Survey EROS Data Centre (1), has been combined with a special dataset for Greenland. The land-cover dataset is based on the processing of two years of 1 km AVHRR data, and is distributed by the US Geological Survey EROS Data Centre (2). The spectrally unfitted orography is obtained by an aggregation of the GTOPO30 data on the model grid. Since the GTOPO30 data comes with an ocean mask (lakes are labelled as land) the land-sea mask is obtained from the 'water' type land-cover dataset. The difference between the 'water' mask and the 'ocean' mask is used to build a 'fresh-water', or 'lake', mask that has been employed as an auxiliary field in the SST analysis for CY21r1 and later cycles.

Apart from being based on the different reference orography data, the computation of the fields in CY21r4 differs from the previous algorithm in a number of ways. The subgrid-scale orography fields are calculated such that the scales below about 5 km do not contribute (these smallest scales will contribute to new roughness-length calculations that are planned for the future). Also, the derivatives needed for computing some of the subgrid fields are equal-area derivatives, and the slope of the resolved model orography is removed from the data before the calculations are applied.

(1) http://edcwww.cr.usgs.gov/landdaac/gtopo30/gtopo30.html
(2) http://edcwww.cr.usgs.gov/landdaac/glcc/glcc.html

Since there are substantial differences from the previous subgrid-scale fields, especially for the slope (which is sometimes larger by up to a factor of three), it was crucial to test thoroughly their impact on the model and to assess the need to adjust the parameters in the associated parametrization scheme. Overall, it was found that the impact of merely replacing the fields was positive in terms of systematic errors in seasonal ensembles of T63 experiments, and so it was decided not to try to re-tune the parametrization scheme. The results of tests using the new orography fields in medium-range forecasts showed a positive impact on forecast scores for the Northern Hemisphere and neutral impact for the Southern Hemisphere.

Finally, a further change has been made to correct two small coding errors that were identified as a result of the adaptation of the ECMWF subgrid orography scheme to the new DWD model. No significant impact of these corrections was found either in extended integrations or in medium-range forecasts.

Post-processing of 10 m winds

The observing stations used for the verification of weather parameters are usually located in open areas, whereas the model roughness length is a so-called 'effective roughness' chosen to obtain adequate area-averaged momentum fluxes. However, the momentum flux (and, therefore, also the 'effective roughness' length) is dominated by the rough terrain features (due, for example, to orography and patchy high vegetation). Consequently, the resulting area-averaged 10-m model wind tends to be lower than observed in open sub-areas. In order to convert the model winds to a form that is comparable to typical 10-m wind observations an 'exposure correction' is applied during the post-processing. Prior to CY21r4, the model winds were interpolated (over land only) from the lowest model level (at about 30 m in the L50 model) to a height of 10 m using a local roughness length of 0.03 m, if this is lower than the model roughness length. The idea was that there is a height above the surface (the blending height - set to the height of the lowest model level, for convenience), where the effects of surface heterogeneity have merged. Below the blending height, the wind profile adapts to the local terrain. In the L60 model, with the lowest model level at 10 m, the mechanism of exposure correction is no longer appropriate. Consequently, the blending height has been set to a value of 75 m, independent of the model's resolution. The wind speed is interpolated to this level from the model levels, followed by a further interpolation to the 10-m level using the same local roughness-length assumption as before. However, the wind direction at 10 m is taken to be the same as that of the model wind at the lowest level. Comparisons between 10 m wind speeds forecast by the L50 and L60 models indicate that the results are improved in the L60 model, the wind speeds being, in general, slightly higher and closer to the observations.

The main impacts of the model changes

Cloud cover

The impact of the changes on the model's cloud fields is summarised in Figure 6. This shows the zonal mean of the total, low-level, mid-level and high-level cloud cover taken from 5-day forecasts for the entire month of September 1999 from the L50 model and the CY21R4 system (which was running experimentally at that time). The most obvious change is a marked increase in low-level cloud cover by about 10% occurring at all latitudes. The main cause for this change has been found to be the interaction of the cloud and convection parametrization with the increased boundary-layer resolution. The high-level cloud cover is reduced everywhere, particularly in tropical areas. There is also a slight reduction in mid-level cloud cover. Recent comparisons of the model cloud cover with retrievals using data from the HIRS instrument on board the polar-orbiting satellites indicates that the changes in high-level and low-level cloud cover are improvements. The net effect on total cloud cover is a slight reduction in the tropics and a small increase in the extratropics. The change in vertical structure is, however, much more significant.

Low-level relative humidity

The changes in the treatment of the evaporation of precipitation lead to substantial changes in relative humidity. There is a decrease in the zonal-mean relative humidity of 3% to 5% in the tropical mid-troposphere. The near-surface relative humidity is generally increased by about the same amount. Table 1 shows the background departures of relative humidity at the 2 m height compared with SYNOP observations, as measured in the data assimilation process. Both the mean and the root mean square of the difference between the observations and the model's first guess are shown, averaged over stations in the Northern and Southern Hemisphere and in the tropical belt. It is evident that a dry model bias (positive background departure) has been largely alleviated in all regions together with a reduction in the RMS difference. This indicates that the new model version predicts more realistic values of low-level relative humidity. The higher values of low-level relative humidity lead to a reduction of a positive bias in surface evaporation over much of the tropical and subtropical oceans.

		Summer		Winter	
		Bias	RMS	Bias	RMS
N. Hemisphere	Old	4.2	11.1	1.3	10.6
	CY21r4	2.1	10.3	–0.2	10.6
Tropics	Old	2.4	12.0	1.9	10.8
	CY21r4	0.3	11.0	–0.2	9.7
S. Hemisphere	Old	3.4	13.0	2.4	11.3
	CY21r4	0.8	11.5	1.7	10.2

Table 1: Bias and root mean square (RMS) differences from the background field (observations minus first guess) for 2 m relative humidity (%) for the previous operational system (Old) and the CY21r4 system. The summer results are from six data assimilation cycles in June 1999; the winter results are taken from 16 cycles in January 1999.

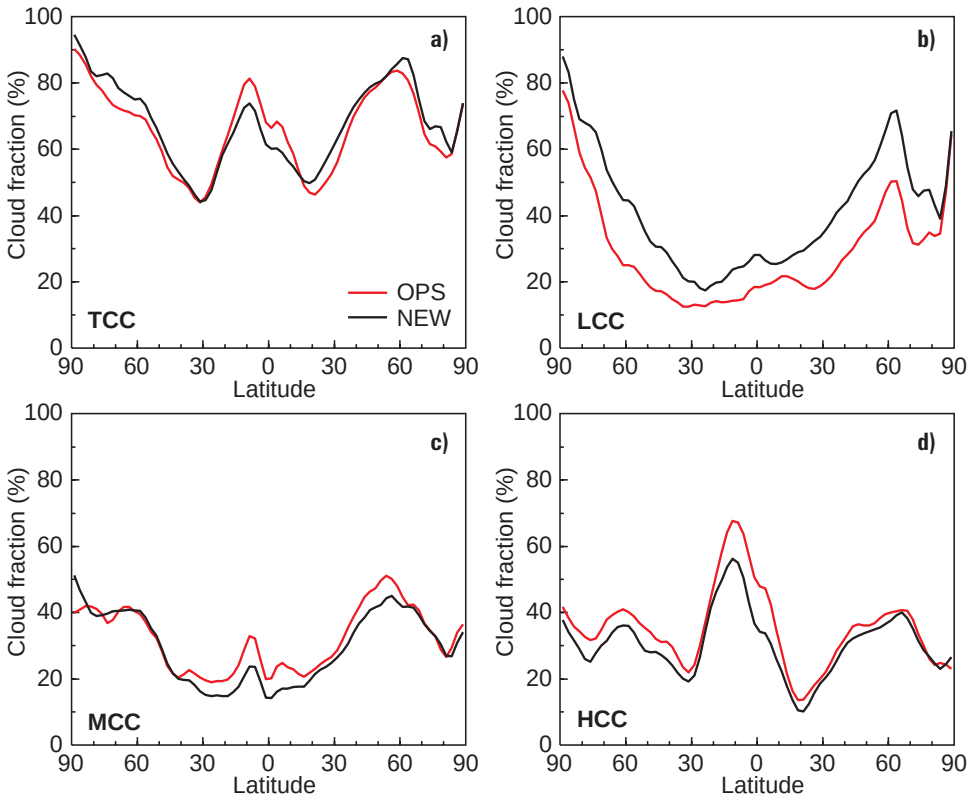

Figure 6: Zonal mean distribution of (a) the total, (b) the low-level, (c) the mid-level, and (d) the high-level cloud cover taken from all 5-day forecasts for September 1999 with the then operational system (red line – OPS) and the new CY21r4 system (black line – NEW).

Tropical temperatures

Another significant impact of the new model is a change in the vertical temperature structure in the tropics. This is summarised in Figure 7, which shows the day-5 forecast temperature error averaged over the entire tropical belt (20°N to 20°S) as a function of pressure for both the old and the new model. An average over 6 forecasts from 14 to 19 June 1999 is shown. It is evident that the warm model bias between 300 and 500 hPa has been largely alleviated and the cold bias above the tropical tropopause has been almost halved.

Precipitation

Figure 8 shows a comparison of the frequency bias of 48-hour forecasts of precipitation over Europe for the entire month of August 1999 with the then operational system (blue) and the new CY21r4 system (red). The frequency bias indicates whether the frequency of a precipitation event larger than a given threshold is well simulated by the model. A value of 1 indicates the correct prediction of the frequency of the event, larger values indicate an overestimation and smaller numbers indicate an underestimation. The precipitation thresholds chosen are 0.1, 1, 2, 4, 8 and 16 mm/day, respectively. The new forecasting system improves the forecasts for all threshold classes, except for those larger than 8 mm/day. Both the overestimation in all classes up to 2 mm/day and the underestimation in the class above 16 mm/day are reduced with the new system.

Summary of improvements to the forecasting system

The entire set of changes described in the above sections has been combined to form the new cycle CY21r4 of the IFS, and extensive testing of its forecast performance has been carried out. Figure 9 shows the 500 hPa geopotential height anomaly correlation scores averaged over 131 forecasts from 6 May to 26 September 1999 for Europe, the Northern Hemisphere and the Southern Hemisphere. The scores indicate a substantial improvement of the forecasting system especially over Europe and the Northern Hemisphere. This result is particularly encouraging, since the forecast performance of the previous operational system over that period included spells of rather poor forecast skill in May and August. Other benefits of the new forecasting system can be summarised as:

- better use of observations in the data assimilation system through improved background error statistics and satellite bias correction schemes;
- better analysis of low-level winds through the use of SSM/I wind-speed retrievals;
- more realistic orography fields;
- improved forecasts of low-level cloudiness, low-level relative humidity, precipitation and 10 m wind speed;
- improved vertical temperature structure in the tropics.

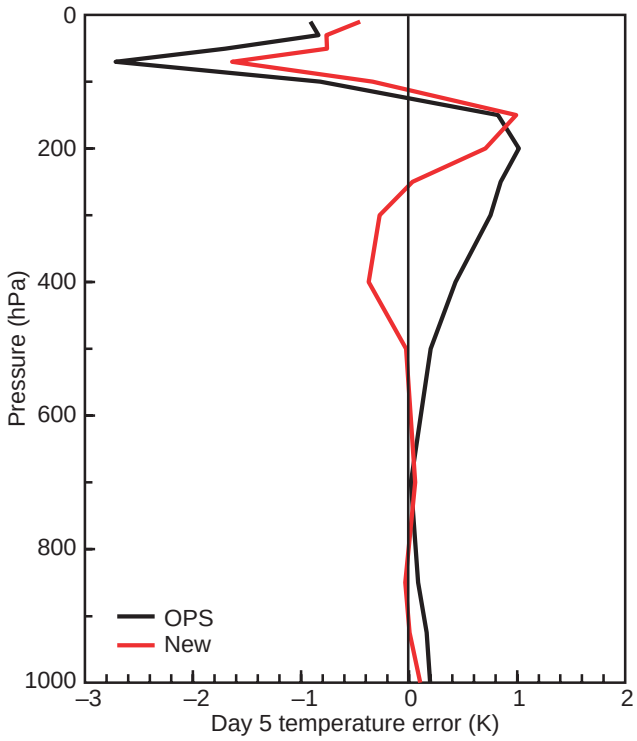

Figure 7: Vertical profiles of the day-5 temperature errors for forecasts from 14 to 19 June averaged of the tropical belt (20°N to 20°S) for the previous operational system (black line-OPS) and the CY21r4 system (red line-New).

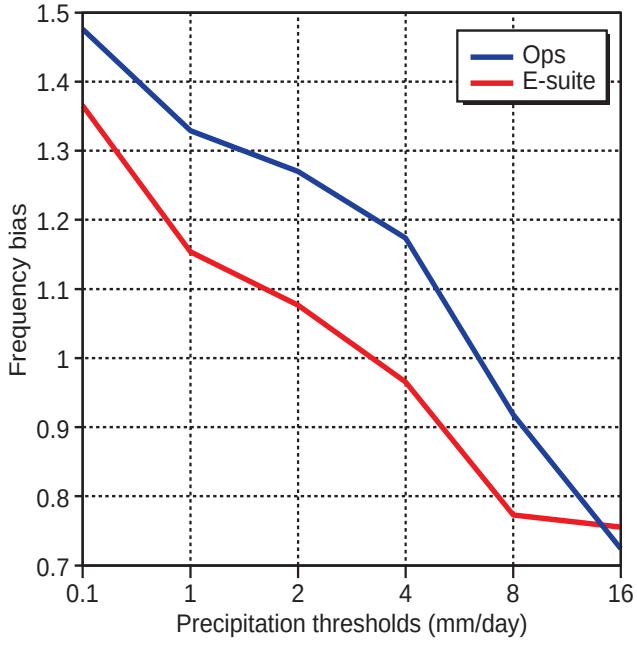

Figure 8: Frequency bias for 48-hour forecasts of precipitation categories larger than 0.1, 1, 2, 4, 8 and 16 mm/day averaged over Europe for the previous operational system (blue line) and for the CY21r4 system (red line).

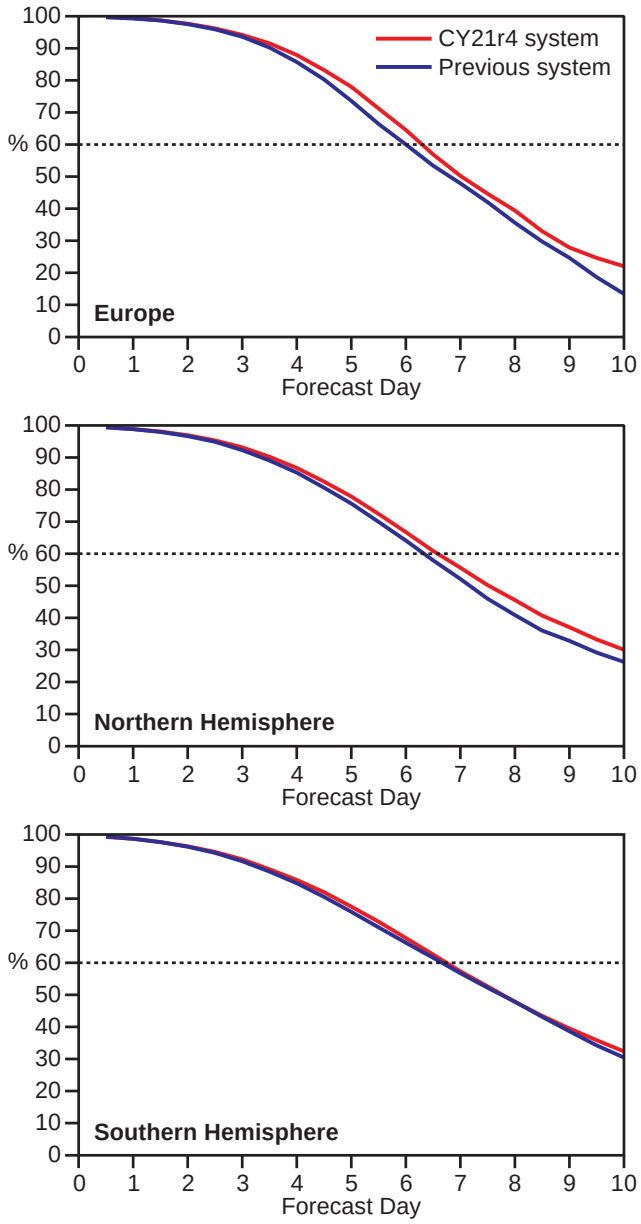

Figure 9: Anomaly correlation scores of the 500 hPa geopotential height for 131 forecasts from May to September 1999 carried out with the previous operational system (blue line) and the CY21r4 system (red line). The areas shown are Europe (top), Northern Hemisphere (middle) and Southern Hemisphere (bottom).

References

Buizza, **R.**, **Miller**, **M.** and **Palmer**, **T.N.** (1999) Stochastic representation of model uncertainties in the ECMWF ensemble prediction system. *Q. J. R. Meteorol. Soc.*, **125**, 2887-2908.

Buizza, **R.** and **Palmer**, **T.N.** (1999) Ensemble data assimilation. Proceedings of the AMS 17th conference on weather analysis and forecasting, 13-17 September 1999, Denver, 231-234.

Jakob, **C.** and **Klein**, **S.A.** (1999) The role of vertically varying cloud fraction in the parametrization of microphysical processes in the ECMWF model. *Q. J. R. Meteorol. Soc.*, **125**, 941-965.

Jakob, **C.** and **Klein**, **S.A.** (1999) A parametrization of the effects of cloud and precipitation overlap for use in general circulation models. ECMWF Tech. Memo. 289.

Teixeira, **T.** (1999) The impact of increased boundary layer vertical resolution on the ECMWF forecast system. ECMWF Tech. Memo. 268.

Untch, **A.**, **Simmons**, **A.** and colleagues (1998) Increased stratospheric resolution in the ECMWF forecasting system. ECMWF Newsletter 82, Winter 98/99, 2-8.

C. Jakob, E. Andersson, A. Beljaars, R. Buizza, M. Fisher, E. Gérard, A. Ghelli, P. Janssen, G. Kelly, A.P. McNally, M. Miller, A. Simmons, J. Teixeira and P. Viterbo

Verifying precipitation forecasts using upscaled observations

Verification of precipitation forecasts against SYNOP observations might seem a pretty straightforward procedure, but providing an interpretation of the results is a very difficult task. The model predicts precipitation fluxes over areas of the order of 60 x 60 km^2, while SYNOP stations report values from rain gauges that typically represent areas of a few tens of cm^2. It is not simple to bridge this gap, as it cannot be claimed that the spectrum of precipitation field drops to zero for scales below 60 km.

A well-posed verification problem is formulated when several local observations of the precipitation flux inside each model grid box are considered. These observations can be obtained from a high-resolution observing network, or from calibrated radar data. A simple hypothesis is to consider each of these observations equally likely to contribute to the precipitation flux in a grid box, as there is usually no information on how large the area that each of them represent is. The 'upscaling' as defined in this study consists of averaging all the observations in a model grid box. The super-observations resulting from this procedure are expected to be representative of the grid box.

In this paper the two approaches (using local and upscaled observations) are compared using both error maps and classical threat scores. Local observations are restricted to those received in real time at ECMWF (SYNOP data available on the GTS) while upscaled observations come from a special dataset obtained from Météo-France.

Météo-France has made available climatological precipitation data for 1997, following a request from ECMWF. The

dataset contains 24-hour accumulated rainfall (the accumulation periods start at 6 UTC) for about 4,390 meteorological stations (synoptic, automatic and climatological) covering the French territory. Each station of the high-density French network is assigned to its closest model grid point, and a simple average of their precipitation reports is then calculated. Mean values, referred to as 'super-observations', are assigned to the grid points themselves. More complicated averaging methods could have been used but it was thought that, as a preliminary test, a simple average would be sufficient to give some understanding concerning the different approaches to precipitation verification.

The precipitation values obtained from the SYNOP stations available on the GTS are accumulated over a 24-hour period from 6 UTC, hence providing a comparable dataset of observations, hereafter referred to as 'SYNOP observations'. In order to compare the SYNOP data with the forecast values, four grid points surrounding each station location were chosen and the values at these grid points linearly interpolated to the station location itself.

The ECMWF model's horizontal resolution in 1997 was T213 with 31 levels in the vertical. The mass-flux convection scheme could distinguish between deep, shallow and mid-level convection, and moisture convergence was used as the deep-convection closure. A more detailed description of the parametrization can be found in Tiedtke (1989).

It is important to note that while the forecast model is the same in the two verification approaches, the observed sample size is different. Typically the sample size of the set of 'upscaled' observations is larger than that of the dataset consisting only of the SYNOP data available on the GTS.

Verification Scores

Contingency tables (in the format of Table 1) for different thresholds have been built for both the 'super-observation' and 'SYNOP observation' datasets. The precipitation thresholds chosen for this study were 0.1, 1, 2, 4, 8 and 16 mm / 24 hours. The Frequency Bias Index (FBI), the Equitable Threat Score (ETS) and the Hansen-Kuiper Score (TSS) have been used to compare the two verification approaches. A detailed explanation of such scores can be found in Wilks (1995). The ETS (L. S. Gandin and A.H. Murphy 1992) is a modified version of the Threat Score rendered equitable by taking away the random forecast (R(a)).

	Observed YES	Observed NO
Forecast YES	a	b
Forecast NO	c	d

Table 1: Contingency table for observed and forecast precipitation categories. The symbols a, b, c and d are referred to in the text.

Using the notation for a, b, c, and d given in Table 1, the FBI is written as:

$$FBI = \frac{a+b}{a+c}$$

The ETS is written as follows:

$$ETS = \frac{a - R(a)}{a + b + c - R(a)}$$

where:

$$R(a) = \frac{(a+b)(a+c)}{a+b+c+d}$$

Finally, the TSS is:

$$TSS = \frac{ad - cb}{(a+c)(b+d)}$$

It can be shown that the TSS is the probability of detection ($a/(a+c)$) minus the false-alarm rate ($b/(b+d)$).

Precipitation verification results

A crude comparison between the two verification methods is depicted in Figure 1, where the forecast precipitation is shown, together with the observations over France on 10 June 1997. Local effects influence observations from SYNOP stations and, therefore, because of their irregular distribution, care must be taken in assuming similar behaviour in neighbouring areas. In regions where there is a relatively regular distribution of observed values the figure reveals that local isolated phenomena that influence data reported by SYNOP stations are actually observed by other neighbouring stations, giving more confidence in any conclusion that could be drawn. For example, Figure 1(a) shows a station in Lorraine (north of the Alps) indicating 15 mm / 24 h of rain. A quick examination of Figure 1(b) shows that the aforementioned SYNOP station is not isolated but it is an integral part of an area of conspicuously large rainfall, although the value representative of the model scale is closer to 9 mm / 24 h.

Forecast error distributions

The spatial distribution of the forecast error has been analysed to assess the model performance. Forecasts for the range t + 42 to t + 66 were averaged monthly and compared with 'super-observations' and 'SYNOP observations' in order to build monthly maps of forecast error; these are irregularly distributed for the 'SYNOP observations' and evenly distributed when 'super-observations' are used.

Figure 2(a) depicts the mean forecast precipitation for June 1997 together with the mean errors obtained by comparing the forecasts with the 'SYNOP observations', while Figure 2(b) shows the forecast errors relative to the

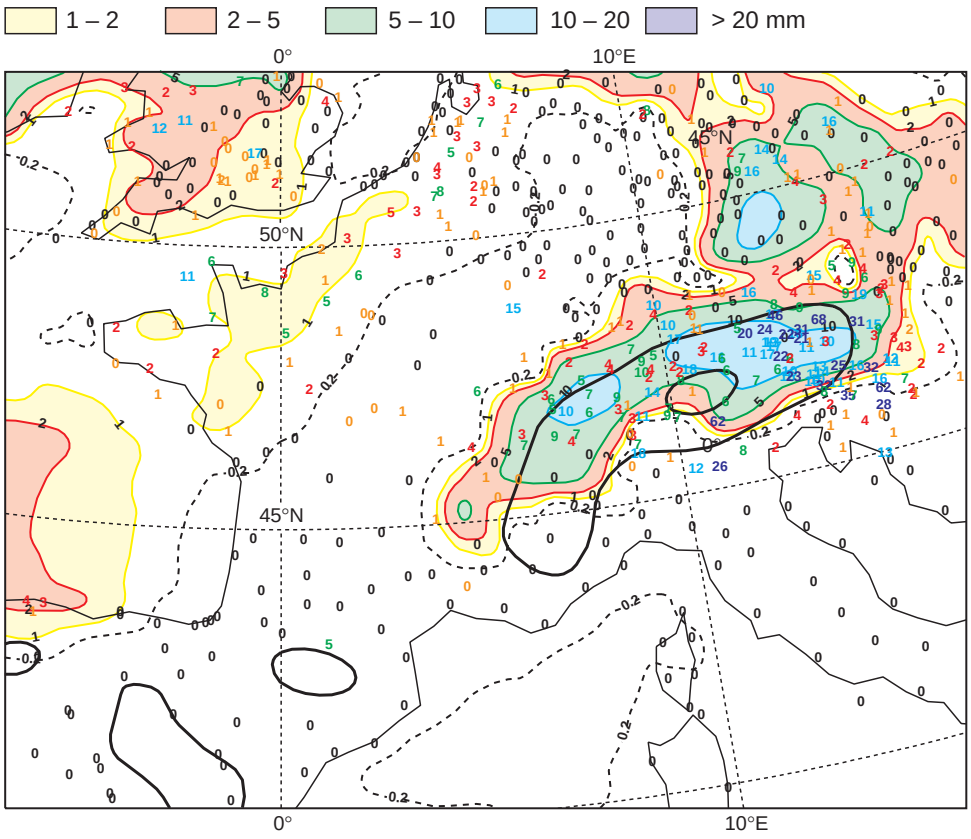

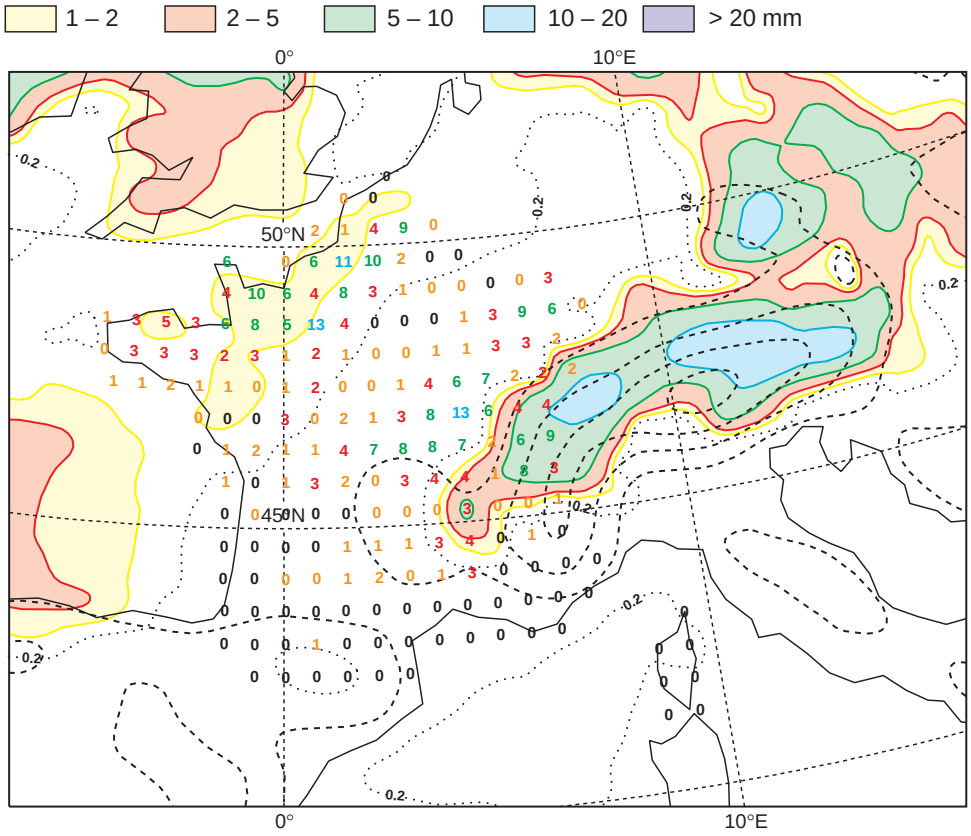

Figure 1: The total precipitation for 06 UTC 13 June 1997. The shaded areas represent the forecast 24-hour rainfall accumulations from t + 42 and the numbers represent the 24-hour accumulated (a) SYNOP observations and (b) 'super-observations'. Colours indicate the ranges of precipitation, as indicated in the legend.

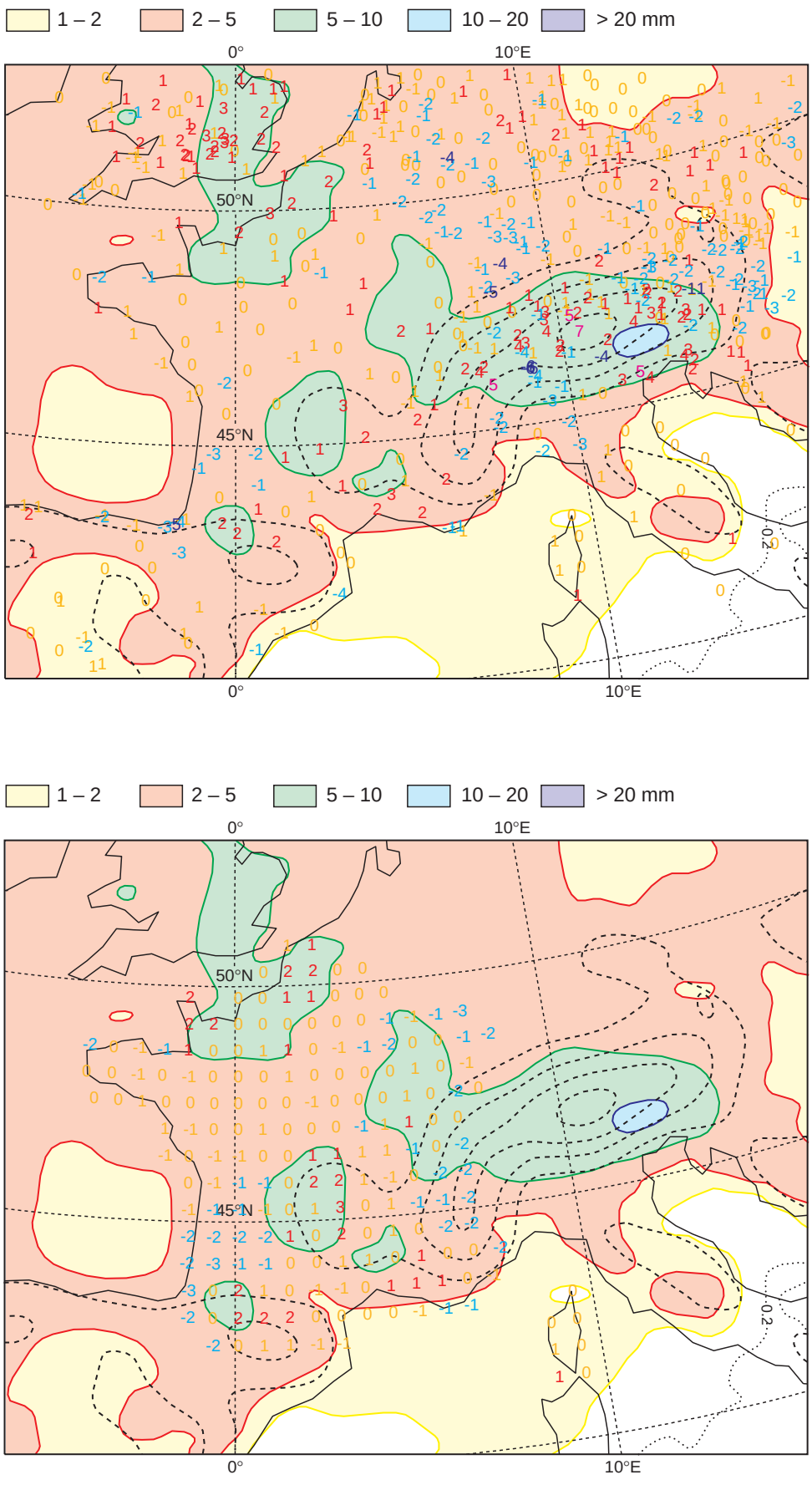

Figure 2: The mean precipitation for June 1997. The shaded areas represent the mean forecast 24-hour accumulated precipitation field from t + 42, and the numbers represent the mean forecast errors calculated using (a) the 'SYNOP observations', and (b) the 'super-observations'. Colours indicate the ranges of precipitation, as indicated in the legend.

'super-observations'. Both maps show that the precipitation amounts are underforecast in areas close to the mountains (north of the Pyrenees, south of the Alps, and the Central Massif) and overforecast in others (south-west of, and over, the Alps). It may be expected that the errors have a flow-dependant signature and, therefore, conclusions on systematic under/over forecasting in certain areas should be drawn with some knowledge of the flow pattern prevailing during the verification period. The monthly averaged analysis of the 700 hPa geopotential height for June 1997 is depicted in Figure 3 and shows a trough over western Europe, France being under the influence of a south-westerly flow. In that context, the underestimation of the precipitation is upstream of the Pyrenees and the Central Massif ranges, and the overestimation is over the mountain range itself. A similar 700 hPa geopotential height pattern can be found May, November and December 1997, and the forecast error distributions for these months indicate again underforecasting of the orographic effects.

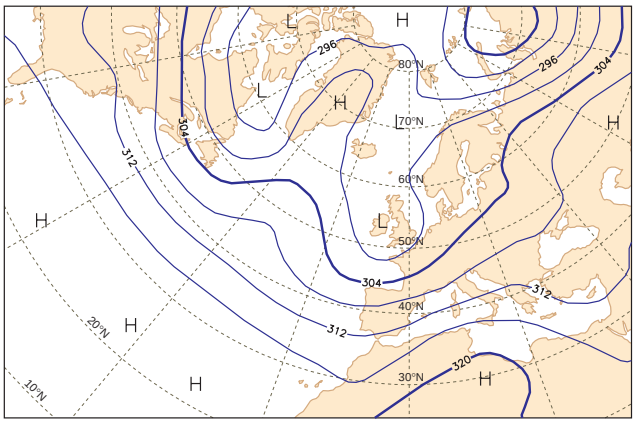

Figure 3: The mean 700-hPa geopotential field for June 1997.

Figure 4 shows the mean forecast precipitation for March 1997 together with the mean errors obtained by comparing the forecasts with the 'super-observations'. A ridge dominates the flow pattern over Western Europe, leading to particularly dry conditions over France. The forecast error is close, or equal, to zero implying a forecast field close to the 'super-observed' pattern of precipitation. Similar conclusions can be drawn for April and September 1997 (not shown). The remaining months have mixed pattern of precipitation, but the model compares well with the 'super-observed' amounts.

Seasonal verification scores

The verification scores for three standard seasons have been examined, namely MAM (March, April and May), JJA (June, July and August), and SON (September, October and November). The forecast range analysed was t+42.

Figure 5 shows a plot of mean forecast values against prescribed precipitation categories of the observations, (a) for spring (MAM), (b) for summer (JJA) and (c) for autumn (SON). The performance of the forecasting system appears to be improved for both small and large amounts of rainfall when verifying against 'super-observations' (red curve closer to the diagonal) in all seasons. A considerable part

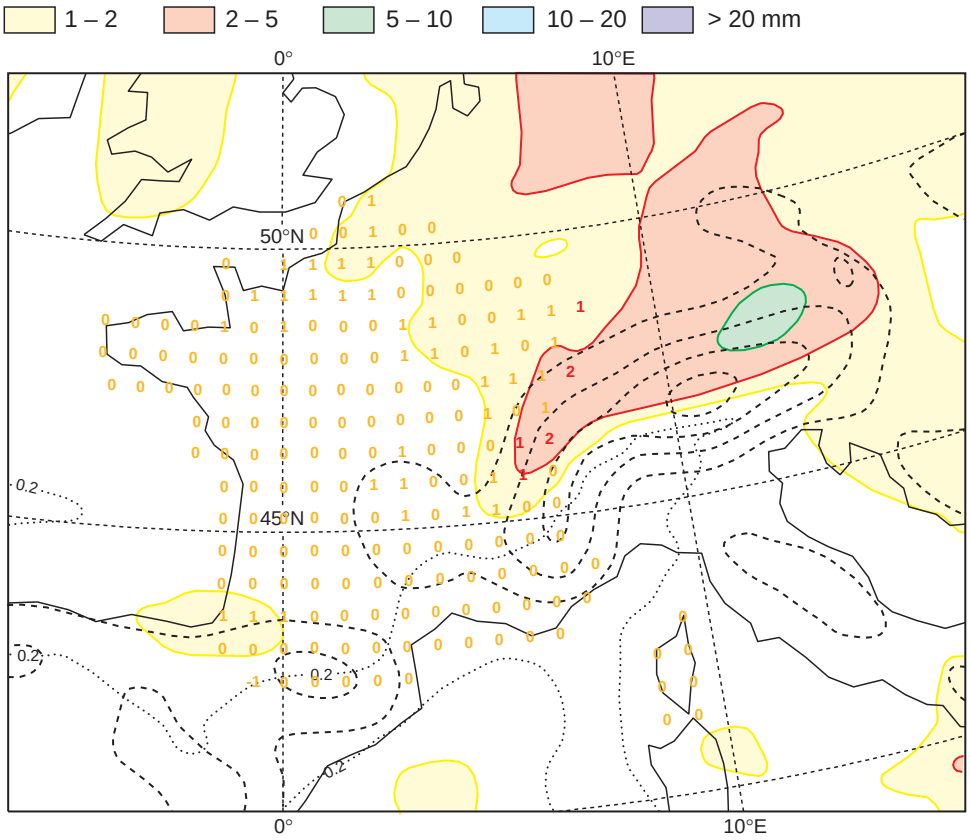

Figure 4: The mean precipitation for March 1997. The shaded areas represent the mean forecast 24-hour accumulated precipitation field from t + 42 and the numbers represent the mean forecast error calculated using 'super-observations'. Colours indicate the ranges of precipitation, as indicated in the legend.

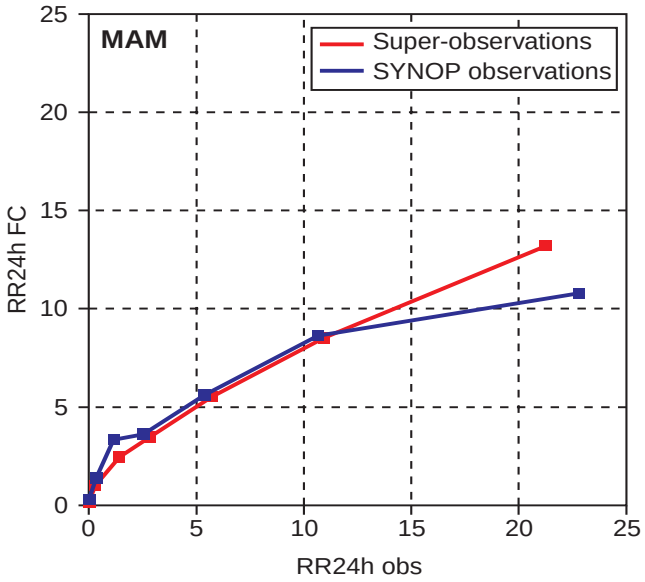

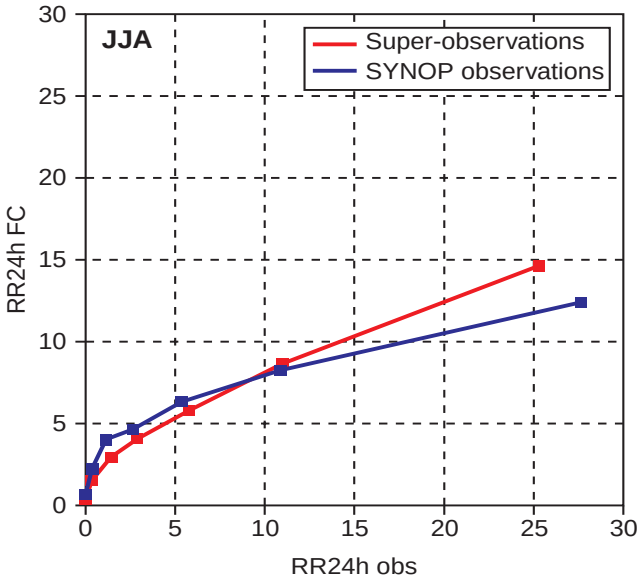

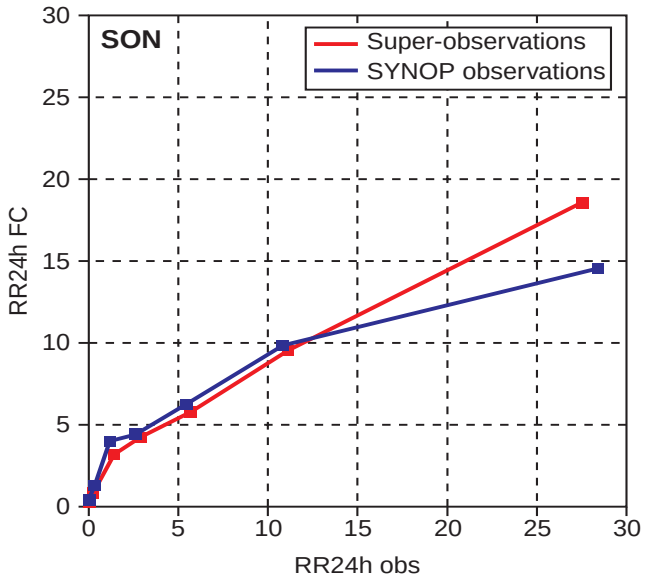

Figure 5: The 1997 seasonal-mean forecast precipitation plotted against the observed precipitation categories for (a) March-April-May, (b) June-July-August and (c) September-October-November. The red curve is for 'super-observations' and the blue curve for 'SYNOP observations'.

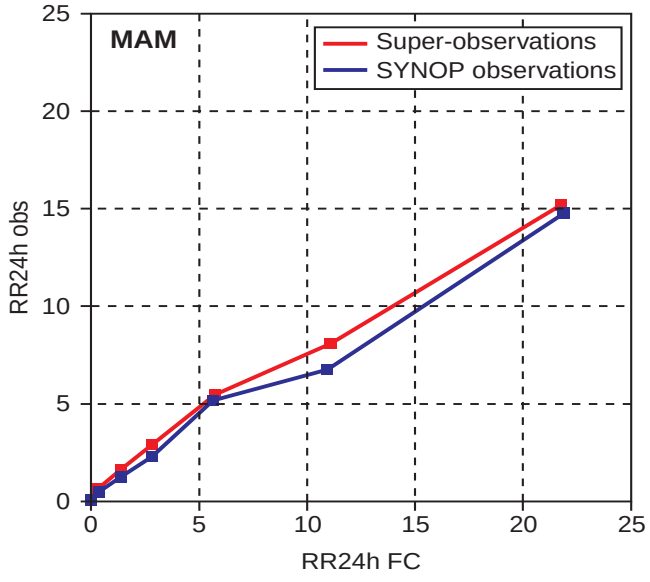

Figure 6: The 1997 seasonal-mean observed precipitation plotted against forecast precipitation categories for March-April-May. The red curve is for 'super-observations' and the blue curve for 'SYNOP observations'.

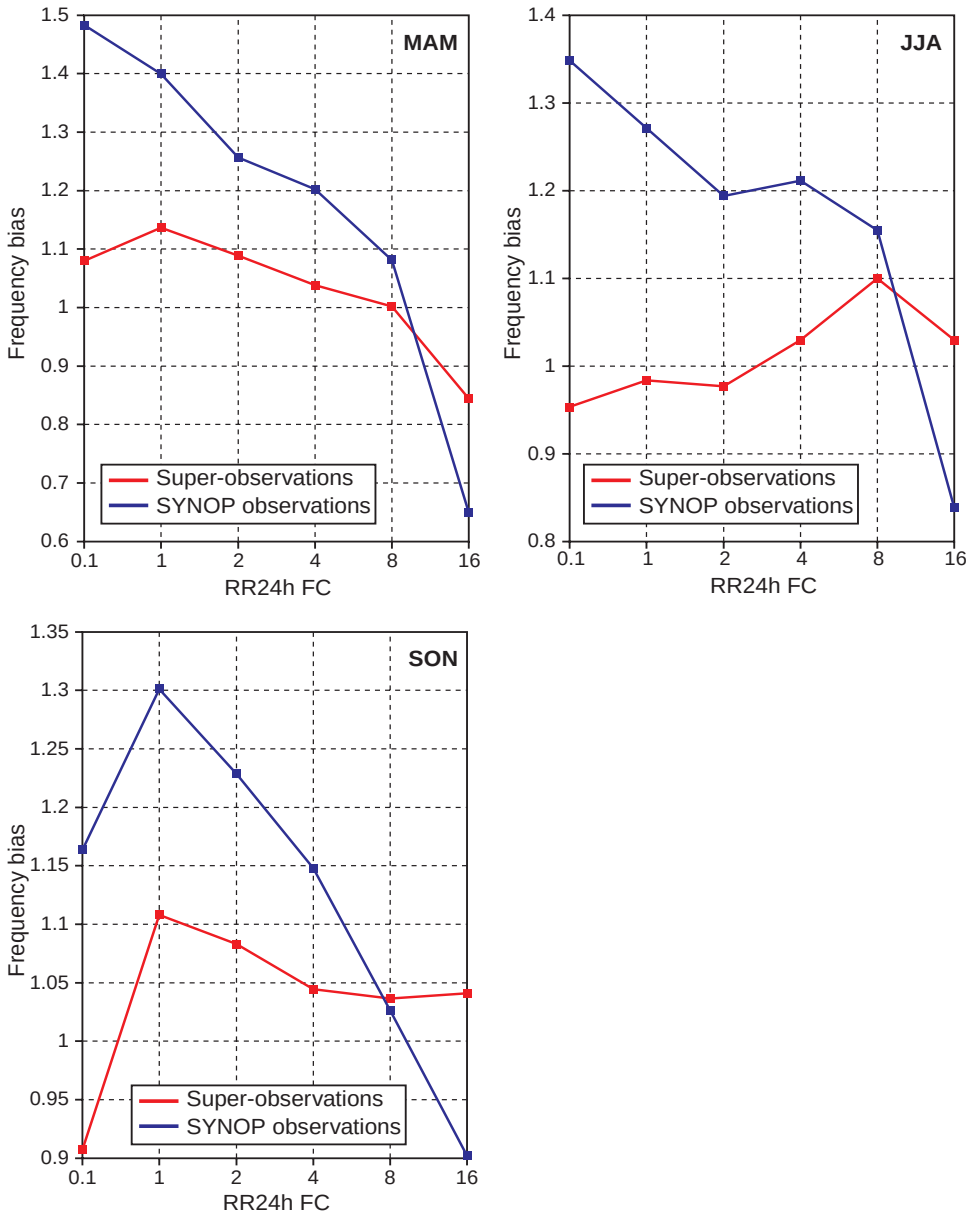

Figure 7: The Frequency Bias Index (FBI) for (a) March–April–May, (b) June–July–August and (c) September–October–November. The red curve is for verification against 'super-observations' and the blue curve for verification against 'SYNOP observations'.

of the error when verifying against local observations is due to 'representativeness' problems. In fact, large amounts of precipitation are not likely to occur over the whole grid area and, therefore, if a local observation is taken to be representative of the area of the model's grid squares the model will appear to perform poorly. In cases of large amounts of rainfall affecting vast areas, then the 'super-observations' are also large and the model verifies better.

Figure 6 depicts a comparison similar to Figure 5, but with the mean observations plotted against given categories of the model precipitation forecasts for MAM. Again the forecast verifies better against 'super-observations' than against SYNOP data. It is interesting to see that any conclusion from this graph alone would point to a positive model bias, while the sign is exactly opposite for Figure 5 (negative bias, or too few cases of strong precipitation). Such behaviour is to be expected when large random errors exceeding the bias signature are present. It is interesting to note that such features are much reduced in the case of super-observations. Similar conclusions can be drawn for JJA and SON.

A dramatic picture appears when the FBI for the two verification methods is compared. Figure 7 depicts the FBI for (a) MAM, (b) JJA and (c) SON. Ideally, if the forecasts were perfect, the FBI should be equal to 1 - that is, the event is forecast exactly as often as is observed. For an FBI greater than 1 the event is forecast more often than observed (overforecast), and vice-versa for FBI less than 1 (underforecast). The FBI is generally much improved when forecasts are compared with 'super-observations' (red curve) than with local observations (blue curve) for all seasons. During the spring the model overforecast the frequency of precipitation cases, with the exception of large-amount categories which were underpredicted. However, the dramatic reduction when going from local to 'super-observations' is an indication that the frequencies of precipitation events occurring locally and of those occurring on the grid scale are very different. Great care

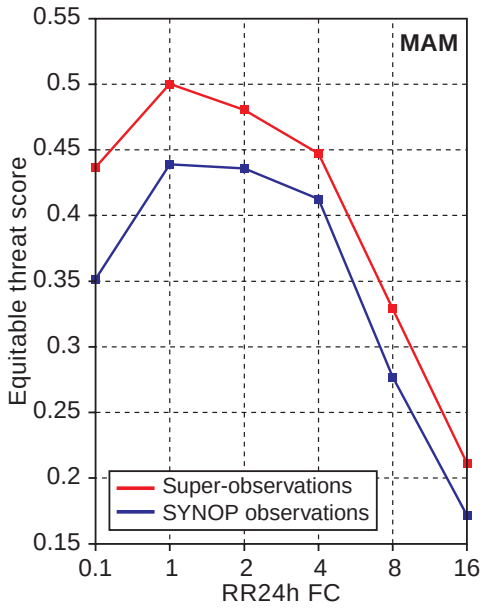

Figure 8: The Equitable Threat Score (ETS) for March-April-May. The red curve is for verification against 'super-observations' and the blue curve for verification against 'SYNOP observations'.

should, therefore, be taken before any conclusion is drawn on the basis of local verification. However, Figure 7 does not indicate whether the bias in the verifications against 'super-observations' are model errors or are errors to be assigned to the aspects of the upscaling method itself (i.e. the limited number of independent observations or the equal weights given to stations with different representativeness).

Figure 8 shows the ETS for MAM. The forecast performance appears to be improved when a comparison is made with the 'super-observations' for all thresholds. Similar behaviour can be found in JJA and SON (not shown).

Figure 9 depicts the TSS for the three seasons. It shows a slightly better performance of the model for small and large amounts of rainfall when the forecast is verified against 'super-observations' for both MAM (Figure 9(a)) and JJA (Figure 9(b)). An overall improvement of the model performance when verified against 'super-observations' is evident for SON (Figure 9(c)).

Summary and concluding remarks

The main drawbacks of the verification method currently used at ECMWF, whereby the SYNOP data available on the GTS are compared with model grid-point values interpolated onto the station location, are the dependency of the results on the interpolation technique used and the disparity between the model's spatial scale and the observation scales. Moreover, the limited number of SYNOP observations available on the GTS implies that some model grid points cannot be verified against any observational data.

The technique of verification against 'super-observations' tries to overcome some of these problems. The information contained in the high-density observation network is 'upscaled' to represent the model spatial scales, thus assuring a fairer comparison with the rainfall forecast. A larger data coverage gives more confidence when analysing forecast error maps to spot possible problems in the forecast model. One of the signatures found in this study, which could not have been derived from the previous (local) verification maps, is the tendency of the model to underestimate the orographic effects on the precipitation fields. This, however, has to be confirmed by further studies.

The scores calculated for the verifications against 'super-observations' have shown that the model performs better than could be anticipated from local observations, particularly in terms of the frequency of occurrence index (FBI). It is interesting to note that, during the summer and autumn, the model underforecast precipitation when compared with 'super-observations' but overforecast small precipitation amounts when SYNOP data were used for the verification.

The efficacy of a regular distributed set of precipitation values representing model spatial scales is also evident in the ETS and TSS results. Both scores show an improved performance of the model when 'super-observations' are used for verifications.

The work described in this paper could be carried on using an extended rainy season for Europe (October to March) to investigate further the model's performance in forecasting rainfall. Model changes could also be assessed using 'super-observations'. If interest is found in Member States, the routine retrieval of 'super-observations' from each Member State on a monthly basis could be envisaged, thereby producing a much more accurate picture of the model's performance.

Examples of applications that are sensitive to large-scale precipitation, such as those forecast by the model, can be found in hydrology (for example, Bremnes et al, 1999). However, the methodology described here is likely to be mainly limited to model validation because end users will usually request forecasts that are representative of smaller areas than the current ECMWF model grid. More work would certainly be needed; however, to develop a European analysis of precipitation that would be truly representative of the model's resolved scales.

References

Bremnes, **B.B.**, **Homleid**, **M.** and **Crochet**, **P**, 1999: Verification of ECMWF Products in Norway. Report 1999 on the Verification of ECMWF products in Member States and Co-operating States, 122-133.

Gandin, **L.S.** and **A. Murphy** 1992: Equitable Skill Scores for Categorical Forecasts. *Mon. Weather Rev.*, **120**, 361-370

Tiedtke, **M.**, 1989: A comprehensive mass flux scheme for cumulus parameterisation in large-scale models. *Mon. Weather Rev.*, **117**, 1779-1800

Wilks, **D.S.**, 1995: Statistical methods in the Atmospheric Sciences. *Academic Press*

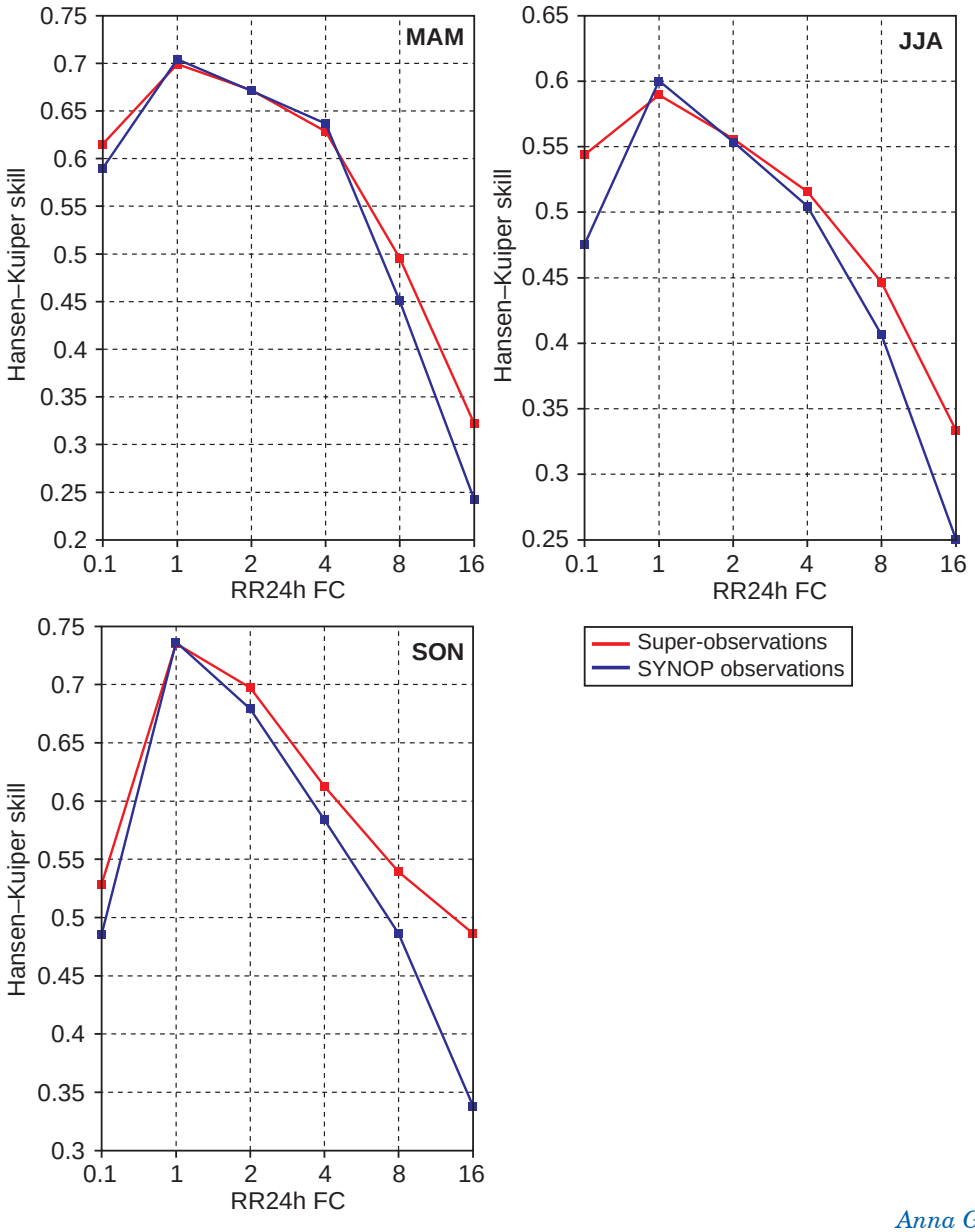

Figure 9: The Hansen-Kuiper Skill (TSS) calculated for (a) March–April–May, (b) June–July–August and (c) September–October–November. The red curve is for verification against 'super-observations' and the blue curve for verification against 'SYNOP observations'.

Anna Ghelli and François Lalaurette

Gigabit Ethernet and ECMWF's new LAN

In September 1992, Dick Dixon wrote in an ECMWF Newsletter article, that the Centre has used computer networks in its operations for many years. In fact, ECMWF networking is as old as ECMWF computing - nearly twenty years. Ethernet was first introduced in 1985 and provided a total bandwidth of almost 10 Megabits. As more and more machines were connected, and were getting more powerful, this bandwidth began to prove inadequate. Hence, during the course of 1992 the Ethernet network was split into segments - more or less corresponding to the office areas (Floor0, Floor1, Floor2, Floor3, etc.) - that were connected via routers to an FDDI backbone or 'core'. In the years following, the splitting of the FDDI backbone, and then the introduction of switching, increased the core bandwidth (up to 1200 Megabits), while in the office areas Ethernet was further segmented; this worked well for a number of years. However, it became clear that this approach would reach its limitations and that more fundamental measures would be required to allow fast data transfers to and from desktop systems and between the servers/supercomputers.

In autumn 1998 a paper stating the requirement for improved bandwidth, reliability, fault tolerance and increased port-density for desktops and servers was presented to the Technical Advisory Committee. ATM and Gigabit Ethernet were identified as the most promising technologies. Following an 'invitation-to-tender' issued in early 1999, ECMWF acquired Cabletron network equipment, based on Gigabit Ethernet and Ethernet 10/100. The new SmartSwitch Routers (SSRs) were then installed

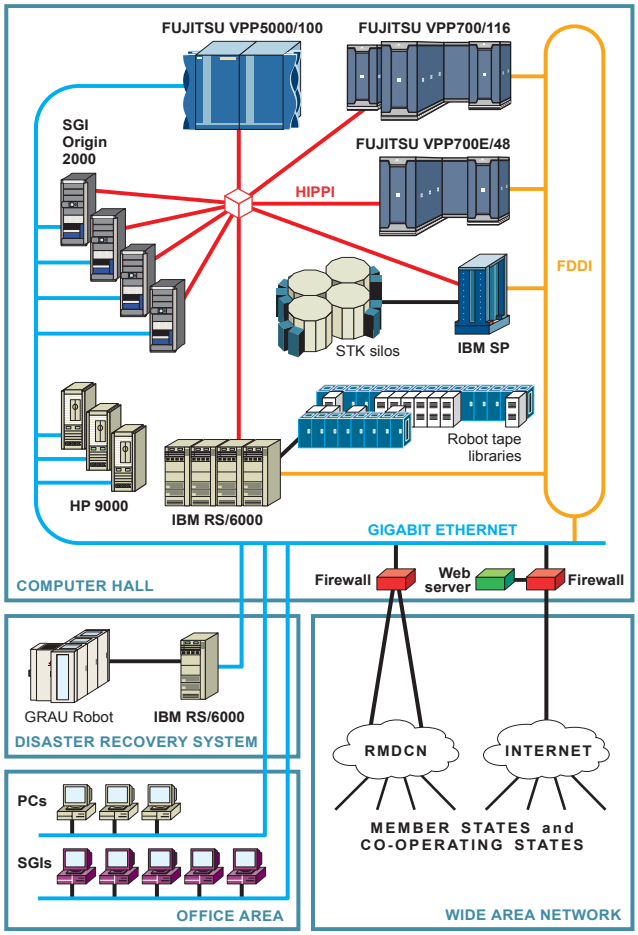

Figure 1: The Centre's computing environment.

Interface description	Gigabit Ethernet		Ethernet 10/100	
	SSR 8600	SSR 2000	SSR 8600	SSR 2000
Links between Core and Edge	18	18	–	–
Links between Core Routers	8	–	–	–
Links between Edge Routers	–	18	–	18
Links to FDDI switches	–	–	8	–
SGI Origin servers	8	–	–	–
HP servers	6	–	–	–
Fujitsu VPP5000	6	–	–	–
DHS servers	2	–	–	–
Links to Firewall	–	–	6	–
NT servers	–	–	4	–
SMS servers	–	–	4	–
User and Operator desktops	–	–	–	18 × 23
Miscellaneous	–	–	10	–
Totals	**48**	**36**	**32**	**432**

Table 1: The port assignments

into the Local Area Network. This equipment now provides a core bandwidth of up to 64 Gigabits.

Constituent parts of the Local Area Network

The Local Area Network interconnects the Centre's computing environment. It can be perceived of as consisting of three parts:

- The *high-speed network* links the Fujitsu VPP supercomputers, the IBM data handling system and the SGI Origin servers via HIPPI routers and switches.
- The *interactive network* links all user and operator workstations and PCs to the servers via routers.
- The *perimeter network* provides the links to the Internet and the Member States via firewalls.

The interactive network

Previously, the interactive network had at its core two FDDI GIGA-switches. Now, the core is built around the two SSR 8600 routers. They are interconnected with a 'trunk' consisting of multiple Gigabit Ethernet links. The Fujitsu VPP5000, Hewlett-Packard, SGI Origin, and some of the IBM DHS servers are connected with Gigabit Ethernet. Where possible, redundant links have been installed. The NT and SMS servers and the firewalls are connected with Ethernet 10/100.

The remaining IBM DHS servers and the Fujitsu VPP700(E) supercomputers do not support Gigabit Ethernet interfaces and are therefore still connected to the FDDI GIGA-switches. Equipping the GIGA-switches with fast Ethernet modules allowed connecting them to the new core with fast Ethernet trunks.

All the user workstations and PCs in the office areas are connected to the network with small SSR 2000 routers. These routers are linked to the core with Gigabit Ethernet.

The SSR routers

In July 1999 two SSR 8600 and twenty SSR 2000 routers were delivered and installed. The SSR 8600s are located in the computer hall and one pair of SSR 2000 routers is located in each of the nine office areas. One pair of SSR 2000s is kept on-site as spares. At the same time the HP high-availability servers and three of the SGI Origin servers were equipped with Gigabit Ethernet interface modules and connected to the new SSR 8600 routers.

After an extensive testing period the new equipment was gradually brought into operation during the month of August 1999. After initial problems the interactive network is now very reliable and without network-related bandwidth bottlenecks. Final acceptance was completed in December 1999. By this time the fourth SGI Origin server, the VPP5000 IOPEs and two of the DHS Athos nodes were also equipped with Gigabit Ethernet interface modules and connected to the SSR 8600 routers.

Both of the Centre's SSR 8600 chassis are fully populated with 24 Gigabit Ethernet ports and 16 fast Ethernet ports. Dual power supplies, dual CPU and dual switching fabrics for resilience, support the network modules.

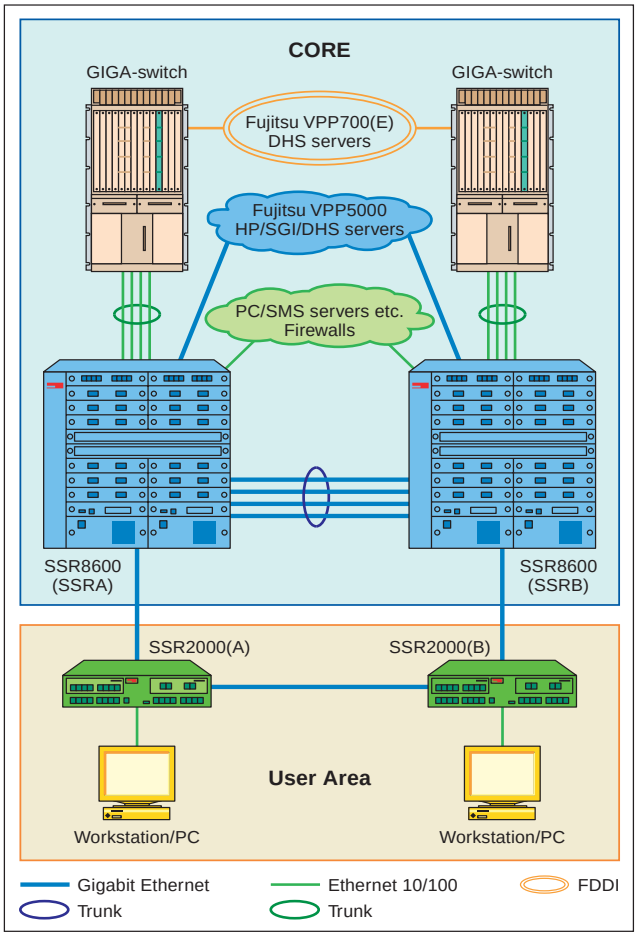

Figure 2: The Centre's interactive network.

The SSR 2000 chassis each contain two Gigabit Ethernet ports and 24 Fast Ethernet ports and a dual power-supply.

There is more to fault tolerance and resilience than having redundant or duplicated hardware. There has to be the network software to support it; all the SSRs run the OSPF routing protocol and VRRP (Virtual Router Redundancy Protocol). Connections through a failing device can be re-routed within a few seconds.

Outlook

The maximum port density has already been reached in the core. Phase 2 of the Gigabit Ethernet installation will increase this capacity in summer 2000 to accommodate new Gigabit Ethernet links, such as to the extended VPP5000.

Dieter Niebel

Ninth ECMWF workshop on the use of high performance computing in meteorology

Every second year the ECMWF hosts a workshop on the use of high-performance computing in meteorology. In 2000 we will hold our 9th workshop in this well established series, from 13 to 17 November. The emphasis of this workshop will be again be on 'TeraComputing', that is, achieving teraflop performance in a production environment.

Our aim is to provide a venue where

- users from our Member States and around the world can report on their experience and achievements in the field of high performance computing and parallel processing during the last two years; plans for the future and requirements for computing power will also be presented;
- vendors of supercomputers are able to talk to managers and end users of meteorological computer centres about their current and future products;
- meteorological scientists can present their achievements in the development of parallel computing techniques and algorithms, and can exchange ideas on the use of supercomputers in future research;
- computer scientists can give an update on their efforts in providing tools which will help users to exploit the power of supercomputers in the field of meteorology;
- the prospects and challenges of creating a computer centre infrastructure for 'TeraComputing' can be discussed

The workshop will consist of a limited number of presentations from speakers, plus a series of 20-minute contributions. As in previous workshops, the morning of the final day will be reserved for an open discussion session. This workshop will start on Monday 13 November at 9:30 am and close on Friday at 12:00 noon. It is planned to publish the proceedings of the workshop.

Attendance at the workshop is by invitation and will be limited to around 100 persons. If you are interested, please contact by post, fax or e-mail:

Norbert Kreitz
ECMWF, Shinfield Park
Reading, RG2 9AX
United Kingdom
Fax: 44 118 986 9450
E-Mail:
NKreitz@ecmwf.int

www:http://www.ecmwf.int/services/training/workshop00.html

Table of Member State and Cooperating State TAC Representatives, Computing Representatives and Meteorological Contact Points

Member State	TAC Representative	Comp. Representative	Met.Contact Points
Belgium	Dr. W. Struijlaert	Mrs. L. Frappez	Dr. J. Nemeghaire
Denmark	Mr. L. Laursen	Mr. N. Olsen	Mr. G. Larsen
Germany	Prof. G.-R. Hoffmann	Dr. E. Krenzien	Mr. D. Meyer
Spain	Mr. T. Garcia Meras	Mr. E. Monreal Franco	Mr. F. Jimenez
France	Mr. E. Legrand	Mrs. M. Pithon	Mr. J. Clochard
Greece	Dr. G. Sakellaridis	Mr. A. Emmanouil	Mr. I. Papageorgiou Mr. P. Xirakis
Ireland	Mr. J. Logue	Mr. P. Halton	Mr. M. R. Walsh
Italy	Dr. S. Pasquini	Dr. G. Tarantino	Dr. G. Maresca
Yugoslavia*			
Netherlands	Mr. A.R. Moene	Mr. H. de Vries	Mr. G. Haytink
Norway	Mr. K. Bjørheim	Ms. R. Rudsar	Mr. P. Evensen
Austria	Dr. G. Wihl	Dr. G. Wihl	Dr. H. Gmoser
Portugal	Mrs. I. Barros Ferreira	Mrs. M.C. Pereira Santos Mr. J.C. Monteiro	Mr. F. Prates
Switzerland	Mr. P. Müller	Mrs. C. Raeber	Mr. R. Mühlebach
Finland	Mrs. K. Soini	Mr. T. Hopeakoski	Mr. P. Nurmi
Sweden	Mr. I. Karro	Mr. R. Urrutia	Mr. O. Åkesson
Turkey	Dr. M. Demirtas	Mr. M. Caglar Mr. N. Yaman	Dr. S. Sari
United Kingdom	Dr. A. Dickinson	Dr. A. Dickinson	Mr. A. Radford

Cooperating States	TAC Representative	Comp. Representative	Met.Contact Points
Croatia	**		Mr. D. Glasnović
Hungary	**		Mr. I. Ihasz
Iceland	Dr. M.Jonsson		Mr. G. Hafsteinsson
Slovenia	**		

* Inactive since 5 June 1992

** The Cooperating States: Croatia, Hungary and Slovenia are represented by the Chairman of the ACCS (Mr. M. Matvijev) who attends the TAC sessions as an observer.

ECMWF publications

Technical Memoranda

No. 284 **Janssen, P.A.E.M.**: On tides in the ECMWF model. December 1999

No. 287 **Hoffschildt, M., J.-R. Bidlot, B. Hansen** and **P.A.E.M. Janssen**: Potential benefit of ensemble forecasts for ship routing. August 1999

No. 288 **Mahfouf, J.-F., A. Beljaars, F. Chevallier, D. Gregory, C. Jakob, M., Janisková, J-J. Morcrette, T. Teixeira** and **P. Viterbo**: The importance of the Earth Radiation Mission for numerical weather prediction. September 1999

No. 290 **Richardson, D.**: Effect of ensemble size on reliability and Brier score. October 1999

No. 291 **Cardinali, C.**: An assessment of using dropsonde data in numerical weather prediction. October 1999

No. 295 **van den Hurk, B.J.J.M., P.Viterbo, A.C.M. Beljaars** and **A.K. Betts**: Off-line validation of the ERA-40 surface scheme. January 2000

No. 296 **Andersson, E., M. Fisher, R. Munro** and **A. McNally**: Diagnosis of background errors for radiances and other observable quantities in a variational data assimilation scheme, and the explanation of a case of poor convergence. November 1999

No. 297 **Barkmeijer, J., R. Buizza, T.N. Palmer, K. Puri** and **J.-F. Mahfouf**: Tropical singular vectors computed with linearized diabatic physics. December 1999

No. 298 **Puri, K., J. Barkmeijer** and **T.N. Palmer**: Ensemble prediction of tropical cyclones using targeted diabatic singular vectors. November 1999

No. 299 **Miller**, **M.**: Resolution studies. September 1999

No. 300 **Chevallier**, **F.** and **J.-J. Morcrette**: Comparison of model fluxes with surface and top-of-the-atmosphere observations. January 2000

Miscellaneous

Chevallier, **F.**: TIGR-like sampled databases of atmospheric profiles from the ECMWF 50-level forecast. *ECMWF/EUMETSAT Numerical Weather Prediction Satellite Application Facility Programme Research Report No. 1.*